Shape-memory Platinum(II) Complexes: Intelligent Vapor-History Sensor with ON-OFF Switching Function

Yasuhiro Shigeta,[a] Atsushi Kobayashi,*[a,b] Tadashi Ohba,[a†] Masaki Yoshida, [a] Takeshi Matsumoto, [c] Ho-Chol Chang, [c] and Masako Kato*[a]

Abstract: A novel Pt(II)-diimine complex, $[Pt(CN)_2(H_2dcphen)]$ (**1**; H_2dcphen = 4,7-dicarboxy-1,10-phenanthroline), was synthesized and its vapochromic shape-memory behavior was evaluated. The as-synthesized amorphous purple solid, $[Pt(CN)_2(H_2dcphen)]\cdot 2H_2O$ (**1P**), exhibited vapochromic behavior in the presence of alcoholic vapors via a transformation to the red, crystalline, porous vapor-adsorbed form, **1R ⊃ vapor**. The obtained **1R ⊃ vapor** complex released the adsorbed vapors upon heating without collapse of the porous structure. The vapor-free, porous **1R ⊃ open** could detect water or *n*-hexane vapor, although these vapors could not induce **1P** to **1R ⊃ vapor** transformation, and **1R ⊃ open** could be easily converted to the initial **1P** by manual grinding. These results indicate that **1** is a new shape-memory material that functions via formation and collapse of the porous framework with emission change upon vapor-adsorption and grinding; this enables it to exhibit *vapor history* and *ON–OFF* switching sensing functions.

Introduction

Sensor materials based on reversible color and/or luminescence changes (chromism) have drawn much attention[1] because these chromic materials facilitate observation of invisible environmental information, *i.e.*, temperature, pressure, and concentration of harmful chemical vapors, via color change of the materials. In particular, vapochromic materials that exhibit color changes upon adsorption/desorption of chemical vapors have attracted considerable attention because of their potential application for sensor devices for detecting vapor from volatile organic compounds (VOCs) which are widely used in our living environments.[2-7] Among the known vapochromic materials, square-planar Pt(II) complexes have been extensively studied in recent decades because they are well-known to exhibit color and luminescence changes based on a structural transformation involving modification of the intermolecular metallophilic interactions.[2-6] The vapor-sensing functionalities of most of the vapochromic materials reported so far are usually based on the color difference between the adsorbed and desorbed forms, as shown in Scheme 1(a). Thus, these materials are suitable for *in situ* detection of chemical vapor, but are not applicable as vapor-*history* sensors, which can memorize the existence of chemical vapor. Such vapor-*history* sensors are very useful and strongly required to ensure chemical safety in living environments. We previously reported the vapochromic behaviors of Pt(II)-diimine complexes, *i.e.*, $[Pt(CN)_2(H_2dcbpy)]$ (**2**; H_2dcbpy = 4,4'-dicarboxy-2,2'-bipyridine; Chart 1)[8] and the corresponding Na salt, $Na_2[Pt(CN)_2(dcbpy)]\cdot 2H_2O$.[3f] It is noteworthy that the Na salt shows interesting vapor-*history* sensing behavior derived from a vapor-induced transformation from the metastable red luminescent amorphous form to the more stable yellow luminescent crystalline form;[3h] however, this color change behavior is irreversible and a dissolution-precipitation cycle is required to clear the history. In order to achieve both *in situ* vapor detection and vapor-*history* sensing, we focused on the shape-memory effect. The shape-memory effect describes materials that undergo shape deformation because of external stimuli, retain the temporary shape when the stimulus is removed, and return to the original shape upon exposure to another stimulus (*e.g.*, heat, light, etc.). Many shape-memory materials have been reported so far in the fields of alloys and polymers.[9] In addition, Kitagawa and co-workers recently reported the shape-memory behavior of a meso-scale porous coordination polymer (PCP) constructed from Cu^{2+} ions and organic bridging ligands.[10] However, most shape-memory materials do not possess appropriate chromophores or luminophores to indicate the shape at the molecular level as color or luminescence, which makes it difficult to easily detect the current shape. The introduction of a chromophore/luminophore with vapor-sensing functionality into shape-memory materials may enable us to create new vapor-sensing materials that can detect chemical vapors not only in real-time, but also record the history of the presence of chemical vapor, as shown in Scheme 1(b).

In this paper, we demonstrate that newly synthesized Pt(II)-diimine complex $[Pt(CN)_2(H_2dcphen)]$ (**1**) (Chart 1; H_2dcphen = 4,7-dicarboxy-1,10-phenanthroline) shows interesting shape-memory behavior in response to vapor adsorption/desorption and mechanical grinding, which is associated with remarkable color and luminescence changes. Complex **1** forms a red luminescent and porous crystalline phase upon adsorption of alcoholic vapors (abbreviated as **1R⊃vapor**) from non-porous amorphous **1P**, and the porous structure is retained without the

[a] Y. Shigeta, Dr. A. Kobayashi, Dr. T. Ohba,[†] Dr. M. Yoshida, and Prof. M. Kato.
Department of Chemistry, Faculty of Science, Hokkaido University
North-10 West-8, Kita-ku, Sapporo 060-0810, Japan
E-mail:akoba@sci.hokudai.ac.jp (Dr. A. Kobayashi)
mkato@sci.hokudai.ac.jp (Prof. M. Kato)
[b] Dr. A. Kobayashi
PRESTO, Japan Science and Technology Agency (JST),
Kawaguchi, Saitama 332-0012, Japan
[c] Dr. T. Matsumoto and Prof. H.-C. Chang
Department of Applied Chemistry, Faculty of Science and Engineering, Chuo University
1-13-27 Kasuga, Bunkyo-ku, Tokyo 112-8551, Japan
[†] Current Address
Institute for Integrated Cell-Material Sciences (WPI-iCeMS)
Kyoto University
Katsura, Nishikyo-ku, Kyoto 615-8510, Japan
[*] This work was supported by JST-PRESTO, a Grant-in-Aid for Scientific Research on the Innovative Area "Artificial Photosynthesis" (No. 2406), (B)(23350025), (C)(26410063), from MEXT, Japan.
Supporting information for this article is given via a link at the end of the document.

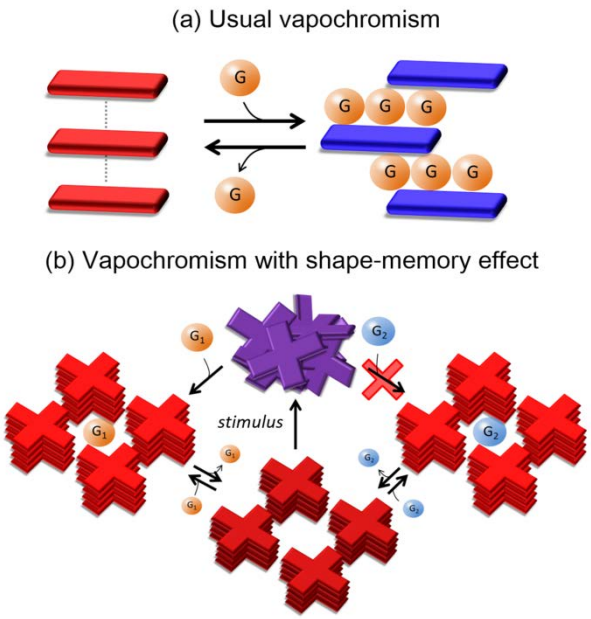

Scheme 1 Schematic diagram of (a) usual vapochromic behavior and (b) new vapochromic behavior with the shape-memory effect reported in this manuscript.

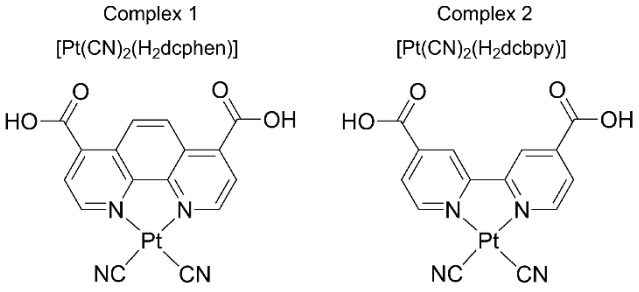

1P and **2P** : Purple-amorphos non-porous phase
1R and **2R** : Red-crystalline porous phase

Chart 1 Schematic molecular structures of complexes **1** (left) and **2** (right).

vapors (abbreviated as **1R⊃open**). In addition, the vapor-desorbed porous phase can detect vapors that cannot induce the structural transformation from **1P** to red-luminescent **1R⊃vapor** via a change of luminescence, and **1R⊃open** is easily converted to the initial purple **1P** upon manual grinding. Although many vapochromic materials have been reported so far, to the best of our knowledge, this is the first vapor-sensing material with shape-memory behavior that may enable us to create more intelligent chemical sensing devices.

Results and Discussion

Crystal structure of 1R⊃water

We successfully synthesized single crystals of **1** in the trihydrated form by CH_3COOH vapor diffusion into a basic

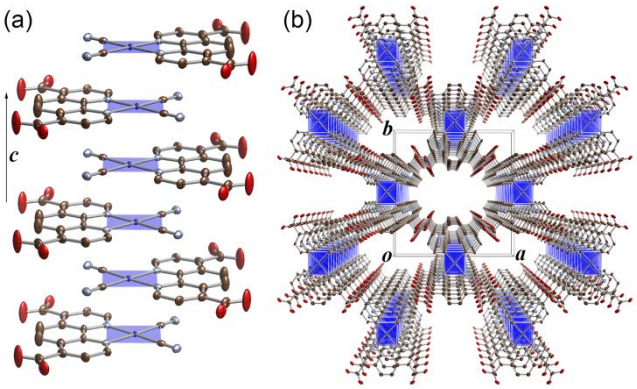

Fig. 1 (a) One-dimensional stacking structure and (b) porous structure of the **1R⊃water** viewed along the *c* axis. Hydrogen atoms and solvent molecules are omitted for clarity.

aqueous solution of the amorphous-like purple solid, **1P** (see the Experimental section). Figure 1 shows the crystal structure of **1R⊃water**, and selected bond lengths and angles are listed in Table S2. As expected from the similarity of the molecular structures of **1** and **2**, the phenanthroline complex, **1R⊃water**, was found to be isomorphous to the bipyridine complex, **2R⊃water** (Figure S1). The central Pt(II) ion features typical square-planar coordination geometry with coordination to two nitrogen atoms of H_2dcphen and two carbon atoms from the cyanide ligands. All the atoms of this complex are located on the same *ab* plane. The bond lengths around the Pt(II) ion, *i.e.*, Pt–C (1.960(5) Å) and Pt–N (2.041(4) Å), are almost equal to those in **2R⊃water**. The two C–O bond lengths of the carboxyl group are very different (1.304(9) and 1.201(8) Å), indicating that the O(2) atom with the longer C–O bond is protonated. Judging from the O(2)–H···N(3) distance (2.652(7) Å) between the protonated carboxyl group and cyanide ligand of the adjacent molecule, relatively tight hydrogen bonds formed between these functional groups. As a result, the two-dimensional hydrogen-bonded network was constructed in the *ab* plane. On the other hand, the fully planar Pt(II) complex molecules are stacked along the *c* axis in an antiparallel orientation to cancel out the dipole moment of each molecule, as shown in Figure 1(a). The intermolecular Pt···Pt distance (3.2355(3) Å) is slightly longer than that of **2R⊃water** (3.2161(6) Å), but remain significantly shorter than twice the van der Waals radius of the platinum atom (3.50 Å), indicating that the metallophilic interaction is effective in this 1D stacked structure. Notably, the Pt···Pt···Pt stacking angle (166.73(1)°) is ~5.2° smaller than that of **2R⊃water** (171.89(2)°), suggesting that the π–π stacking interactions in **1R⊃water** are more effective than those in **2R⊃water**, resulting in the formation of a more twisted 1D zig-zag chain structure. As shown in Figure 1(b), 1D large porous channels formed along the *c* axis, and the pore size was estimated to be about 6.4 × 6.8 Å, which is smaller than that of **2R⊃water** (6.1 × 8.8 Å). Single crystal X-ray structural analysis also revealed that this crystal contains at least three hydrated water molecules per Pt(II) complex molecule in the pores. By using the SQUEEZE program, the void fraction of **1R** was estimated to be 35.2% in the unit cell,

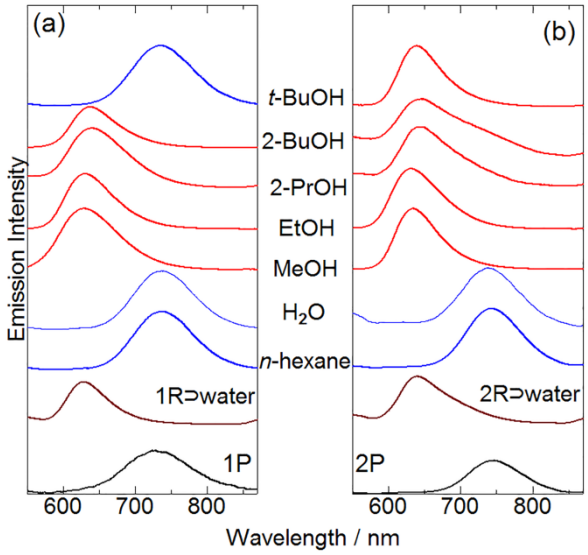

Fig. 2 Changes of the luminescence spectra of (a) **1P** and (b) **2P** after exposure to various solvent vapors at 30 °C for five days (λ_{ex}= 400 nm). Spectra of red crystalline **1R⊃water** and **2R⊃water** are represented by brown solid lines. Observed spectra similar to that of initial **1P** (**2P**) or red-crystalline **1R⊃water** (**2R⊃water**) are shown as blue or red lines, respectively.

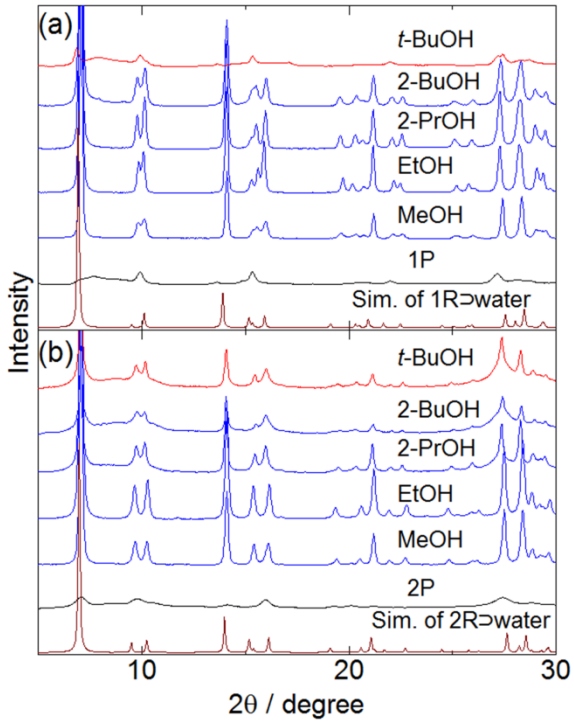

Fig. 3 Powder X-ray diffraction patterns (λ = 1.5385 Å) of amorphous purple powders of (a) **1P** and (b) **2P** upon exposure to several alcoholic vapors. Each bottom line shows the simulated pattern calculated from the crystal structure at 100 K. The exposure time for each vapor was five days at 30 °C. Observed patterns similar to the simulation of **1R⊃water** (**2R⊃water**) are shown as blue lines.

which is also smaller than that of **2R** (39.5%) (note: the hydrated water molecules in the pore were excluded in these calculations); this is due to the larger molecular volume of the H_2dcphen ligand than that of H_2dcbpy.

Multichromic Behavior

We previously reported the vapor-induced color/luminescence change behavior of **2P**.[1c,10] In this work, we examined the vapochromic behavior of **1P** because of the isomorphous structures of **1R⊃water** and **2R⊃water**. Figure 2 shows changes in the emission spectrum of **1P** under exposure to several kinds of vapors for five days in comparison with that of red-crystalline **1R⊃water**. The observed emission maxima for both complexes are summarized in Table S3. The initial purple solid, **1P**, shows weak luminescence at 733 nm, which is at a 11 nm shorter wavelength than that of bipyridine complex **2P**. Interestingly, bright red luminescence centred at around 630 nm was observed after exposure of **1P** to MeOH, EtOH, 2-PrOH, and 2-BuOH vapors for five days at 303 K, as shown in Figure 2(a). It is noteworthy that the emission maxima for these vapor-exposed samples are very close to that observed for red crystalline **1R⊃water**, suggesting that the emission can be attributed to the ^{3}MMLCT (triplet metal-metal- to-ligand charge transfer) transition state generated by effective Pt-Pt interactions. In contrast, no change was observed under exposure of **1P** to non-polar organic vapors, such as *n*-hexane (see Figures S2 and S3). Very similar luminescence changes under exposure to alcoholic vapors were also observed for bipyridine complex **2P**, as reported previously.[1c] A remarkable difference between these two complexes was observed in *t*-BuOH vapor: Although the emission maximum of **2P** changed to 638 nm after exposure to *t*-BuOH vapor, the spectrum of **1P** did not change at all. Considering that both complexes show bright red emission centred at around 640 nm under exposure to 2-BuOH, both the bulky *t*-Bu group of *t*-BuOH vapor and the smaller pore size of **1R** may be plausible explanations for why **1P** did not change under exposure to *t*-BuOH vapor.

To elucidate the origins of the luminescence changes of **1P** in the presence of alcoholic vapors, powder X-ray diffraction (PXRD) patterns were measured for vapor-exposed **2** and **1**. As shown in Figure 3, **1P** and **2P** showed very broad patterns, indicating that these purple solids are almost amorphous. After exposing these amorphous-like solids to alcohol vapor, dramatic changes were observed in the luminescence spectra. The observed PXRD patterns of **1** and **2** exposed to MeOH, EtOH, 2-PrOH, and 2-BuOH were almost identical to the simulated patterns calculated from the crystal structures of **1R⊃water** and **2R⊃water**, respectively. These results indicate that a vapor-induced amorphous-crystalline transformation occurred in the presence of these alcoholic vapors to form vapor-adsorbed porous phases of **1R⊃vapor** and **2R⊃vapor** with effective Pt⋯Pt interactions. TG-DTA analysis and vapor- adsorption

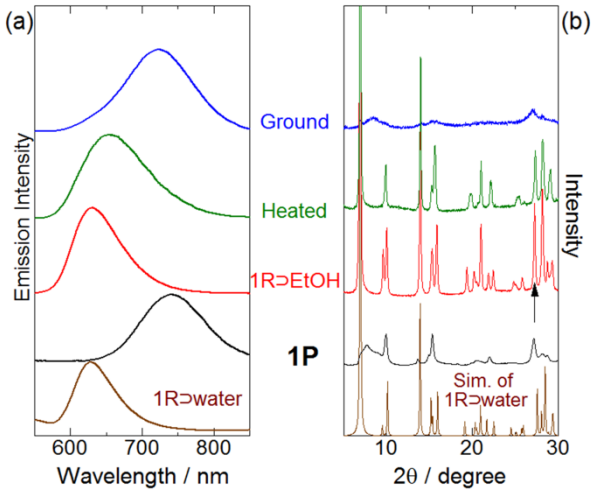

Fig. 4 Changes in the (a) luminescence spectra (λ_{ex}= 400 nm) and (b) powder X-ray diffraction patterns (λ= 1.5418 Å) of **1R⊃EtOH** (red), **1R⊃EtOH** after heating (green), and **1R⊃EtOH** after heating and grinding (blue). The black lines in both panels show the emission spectrum and PXRD pattern of **1P**. The bottom pattern in (b) is the simulated pattern calculated from the crystal structure of **1R⊃water**. The arrow in (b) indicates the position of the (002) reflection.

isotherm measurements revealed that these two Pt(II) complexes adsorbed the alcoholic vapors (see below and Figure S4). As a result, the luminescence maxima of vapor-adsorbed **1R⊃vapor** and **2R⊃vapor** are very similar to those of **1R⊃water** and **2R⊃water**, respectively (Figures 2(a) and 2(b)). The PXRD patterns under exposure to *t*-BuOH vapor also show a very clear difference between the behavior of **1P** and **2P**: The PXRD pattern of phenanthroline complex **1P** only showed a negligible change under exposure to *t*-BuOH vapor, while that of bipyridine complex **2P** after exposure is almost identical to the simulated pattern of **2R⊃water**. This difference is attributed to the differences in the pore sizes: The larger pores of bipyridine complex **2R** (~6.1 × 8.8 Å^2) than those of phenanthroline complex **1R** (~6.4 × 6.8 Å^2) enable **2R** to adsorb *t*-BuOH vapor, resulting in large changes of both the emission and PXRD spectra in the presence of *t*-BuOH vapor. On the other hand, the PXRD patterns of both **1P** and **2P** were not affected by exposure to non-polar vapor and water vapor (Figures S5 and S6). Considering that the porous structures of these complexes are supported by a 2D hydrogen bonding network consisting of hydrophilic carboxyl and cyanide groups, the non-polar vapors did not adsorb into the pores because of their low polarity. Although water molecules have large dipole moments, the structural transformation from **1P** to **1R⊃vapor** was not observed; this implies that a certain molecular volume of the vapors is required to trigger the transformation. It is also noted that the transformation was hardly observed under exposure to 1,1,1-trichloroethane vapor which has almost the same molecular shape and volume to that of *t*-BuOH (see Figure S7), the hydrogen donating ability of the alcohols is important to trigger the transformation.

We next examined desorption of the adsorbed alcoholic vapors. As shown in Figure 4(a), **1R⊃EtOH** exhibited red luminescence at 630 nm.[11] After desorption of EtOH by heating at 383 K (as confirmed by TG analysis, see Figure S4), the luminescence maximum shifted to 653 nm, which is still remarkably shorter than that of the initial purple solid, **1P**. The observed PXRD pattern after desorption of EtOH by heating is still very similar to that of the EtOH-adsorbed complex and the simulated pattern of **1R⊃water**, indicating that the porous structure of **1R** is retained even after removal of EtOH to form open-channel structures in **1R⊃open**. The diffraction peak observed at about 27°, which was indexed to (002) and corresponds to the direction of the intermolecular Pt-Pt interactions, was negligibly shifted by removal of EtOH (Figure S8). On the other hand, the lattice constant refinements for these PXRD patterns suggest that removal of EtOH significantly affected the *ab* plane rather than the *c* axis (Table S4). Thus, the intermolecular Pt–Pt interactions could be strengthened by EtOH removal probably because of slipping of the planar [Pt(CN)$_2$(H$_2$dcphen)] molecules in the *ab* plane to form more linear Pt–Pt stacking structure, resulting in a red shift of the ^{3}MMLCT emission. Therefore, the porous structure of **1R** can be formed by adsorption of alcoholic vapors into the porous channels to form **1R⊃vapor**, and removal of the guest molecules does not degrade the porous structure of **1R** to give the open-framework of **1R⊃open**; However, it has a significant impact on the intermolecular Pt–Pt interactions via slipping to linearize the Pt–Pt–Pt stacking angle. Interestingly, EtOH-desorbed **1R⊃open** showed dramatic color and luminescence changes upon manual grinding in a mortar, as shown in Figure 4(a): The sample color changed from red to purple and the luminescence band of the ground sample was observed at 724 nm, which is close to that of the initial purple solid, **1P**. In addition, the observed PXRD pattern of the ground sample was very broad. Thus, EtOH-desorbed **1R⊃open** was transformed to weakly emissive purple amorphous-like solid **1P** by manual grinding.[12]

Shape-memory Effect and ON-OFF Switching of Vapochromism

To confirm that the vapochromism was derived from vapor adsorption, we measured the vapor adsorption isotherm of **1** upon exposure to EtOH vapor (Figure 5). The same sample was used continuously, and the pretreatments before the measurements varied. The first measurement was performed on purple amorphous **1P** that had been heated under high vacuum. Although negligible vapor adsorption was observed at a low relative pressure (P/P_0) of <0.4, a large vapor uptake of up to 1.8 mol/mol was observed above P/P_0 = 0.4. The desorption process was clearly different from the adsorption process: The number of adsorbed EtOH molecules slowly decreased, but it still retained 0.9 mol/mol at a very low relative pressure of 8.6 × 10^{-3}. Considering that **1P** transformed to the red crystalline vapor-adsorbed form, **1R⊃EtOH**, under exposure to EtOH vapor, the sharp increase of EtOH vapor uptake at around P/P_0 = 0.4 and large hysteresis between the adsorption and desorption processes likely originate from the structural transformation from

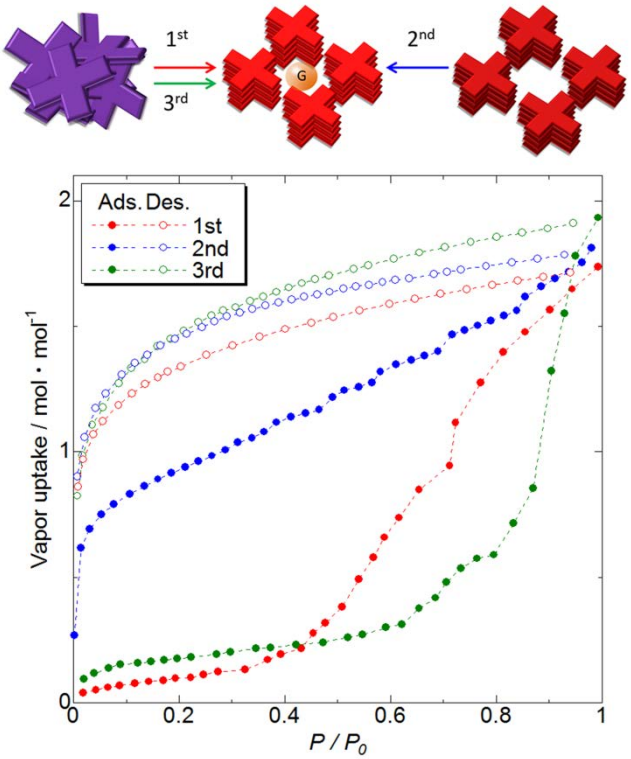

Fig. 5 EtOH-vapor adsorption isotherms of **1** at 298 K with schematic illustrations of adsorption processes. The same sample was used in these three measurements with different pretreatments. Amorphous purple form **1P** was used for the first measurement (red). Before the second measurement (blue), the sample was heated *in vacuo* at 120 °C to obtain vapor-free red crystalline **1R⊃open**. Before the third measurement (green), the sample was heated *in vacuo* at 120 °C and then manually ground in a mortar at room temperature to generate the amorphous purple form, **1P** which was heated again at 120 °C to remove all water adsorbed in the grinding process. Closed and open symbols show the adsorption and desorption processes, respectively.

the non-porous amorphous-like solid, **1P**, to the EtOH-adsorbed porous crystalline solid of **1R⊃EtOH**. The EtOH (about 1 mol/mol) that remains at very low pressure during the desorption process suggests that the adsorbed EtOH molecules were strongly bound in the pore probably by the formation of hydrogen bonds with the carboxyl groups of the porous framework. Next, we recorded the second vapor adsorption isotherm using the same sample as in the first measurement. Before the second cycle, the sample was heated at 120 °C for one day to completely remove the adsorbed EtOH from the pores to obtain vapor-free red crystalline **1R⊃open**. Interestingly, the obtained isotherm was significantly different from the first adsorption isotherm, as shown in Figure 5: In the second isotherm, a large amount of EtOH adsorbed at a very low relative pressure (~0.83 mol/mol at P/P_0 = 0.1). In contrast, the saturated adsorption amount and desorption behavior were almost the same as those in the first cycle. The sharp increase of vapor uptake at very low pressure is characteristic of microporous materials, and indicates that EtOH-desorbed **1R⊃open** contained micropores at the beginning of the second measurement. Therefore, the porous structure constructed by EtOH adsorption (*i.e.*, *gate-opening* behavior) during the first adsorption process could be retained after removal of EtOH by heating during the pretreatment of the second cycle. It should be noted that the purple amorphous form, **1P**, did not convert to vapor-free porous **1R⊃open** under increasing temperature in a vacuum (and *vice versa*; Figures S9 and S10). Interestingly, this characteristic feature of microporous materials observed in the second isotherm completely disappeared in the third cycle in which the sample was heated at 120 °C for one day to remove EtOH and then manually ground in a mortar to completely regenerate amorphous **1P** which again heated *in vacuo* at 120 °C for one day before the third measurement. The observed isotherm in the third measurement was similar to that of the first one with a large hysteresis between the adsorption and desorption processes, indicating that the porous form of **1R**, which was constructed in the first EtOH-adsorption cycle and retained in the second cycle, was broken down by manual grinding to non-porous amorphous **1P** during the pretreatment in the third cycle. These adsorption measurements in the three cycles clearly demonstrate that **1** exhibits shape memory behavior, *i.e.*, this complex can memorize vapor-adsorption history by forming the porous structure, **1R**; this vapor-adsorption history can be retained even after removal of the adsorbed vapors, but can be cleared by removal of the vapor followed by manual grinding to form the non-porous amorphous purple form, **1P**. This intelligent vapor-sensing function based on the shape-memory behavior was also observed for the bipyridine analogue **2** (see Figure S11), suggesting that the lattice stability of the porous structure suitable for this shape-memory behavior could be supported by two-dimensional hydrogen-bonded network in the *ab* plane and the one-dimensional intermolecular metallophilic interaction along the *c* axis.

Next, we examined the vapochromic behavior of the red luminescent porous form, **1R⊃open**, because the hydrogen bond-supported porous framework may be able to adsorb not only the vapors that induce the amorphous–crystalline transformation from **1P** (*e.g.*, MeOH and EtOH), but also the vapors that cannot induce the transformation (*e.g.*, H_2O).Figure 6 shows the relative humidity dependence of the luminescence spectrum of vapor-free **1R⊃open** at room temperature. As discussed above, vapor-free **1R⊃open** prepared by thermal removal of adsorbed EtOH showed an emission maximum at 653 nm at room temperature in air, whereas the emission shifted to shorter wavelengths (633 nm) in 100% RH. On the other hand, it shifted to longer wavelength in lower relative humidity (see Figure 6(b)). In contrast, the luminescence spectrum of the initial non-porous purple form, **1P**, did not change at all under exposure to water vapor (Figure S2). These significantly different results clearly indicate that the blue-shifts of the luminescence of vapor-free **1R⊃open** under exposure to water vapors originated from water vapor adsorption, which should affect the intermolecular metallophilic interactions in the Pt(II)-stacked chain. To elucidate whether the blue-shift of the luminescence of **1R⊃open** originated from H_2O vapor

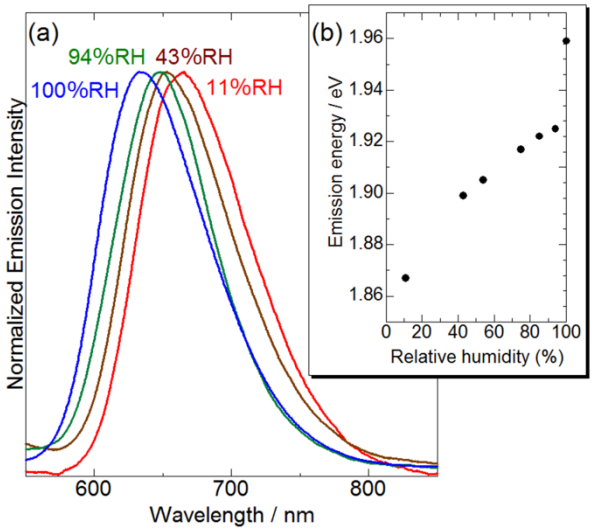

Fig. 6 (a) Relative humidity dependence of the emission spectrum of **1R⊃open** at room temperature (λ_{ex} =400 nm). (b) Relationship between emission energy and relative humidity. Humidity in the quartz cell was controlled by using saturated aqueous solutions of various metal salts.[13]

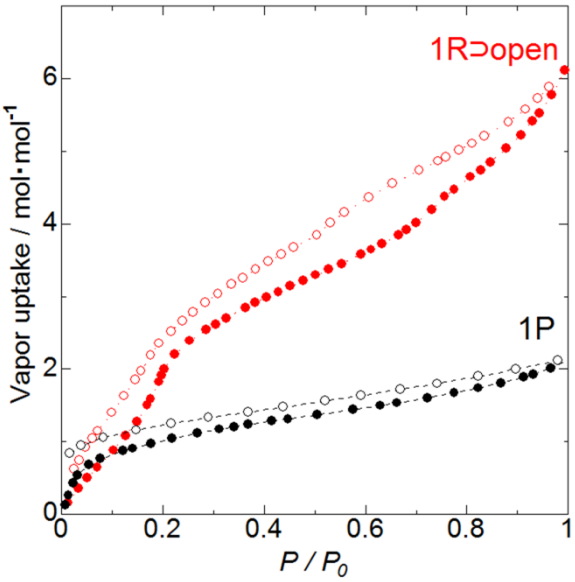

Fig. 7 Water-vapor adsorption isotherms of **1P** (black) and **1R⊃open** (red) at 298 K. Closed and open symbols show the adsorption and desorption processes, respectively.

adsorption, we measured H_2O vapor-adsorption isotherms for both the initial amorphous purple form, **1P**, and the vapor-free form, **1R⊃open** (Figure 7). Each isotherm was measured after heating at 120 °C *in vacuo* to remove all the adsorbed solvent molecules. Interestingly, the saturated adsorption amount of **1R⊃open** (~6.1 mol/mol at P/P_0 = 0.99) was three times larger than that of **1P** (~2 mol/mol at P/P_0 = 0.96). Considering that water-exposed **1R⊃open** has an almost identical structure as **1R⊃water** (Figure S12), this noteworthy difference is likely due to the existence of porous channels in **1R**. In other words, the non-porous amorphous form, **1P**, can adsorb H_2O vapor via the formation of several hydrogen bonds with the hydrophilic carboxyl groups of the dcphen ligands and/or cyanide ligands (*i.e.*, chemisorption). On the other hand, vapor-free **1R⊃open** should be able to adsorb H_2O vapor not only by chemisorption around the hydrophilic groups, but also by physisorption in the porous channels, which enables it to adsorb more H_2O than **1P**. These results indicate that the shape-memory effect based on the gate-opening behavior (*i.e.*, **1P** to **1R⊃open**) enables the vapochromic material not only to record past vapor adsorption, but also detect vapors that could not be detected in the gate-closed *initial* form **1P** (Scheme 2).

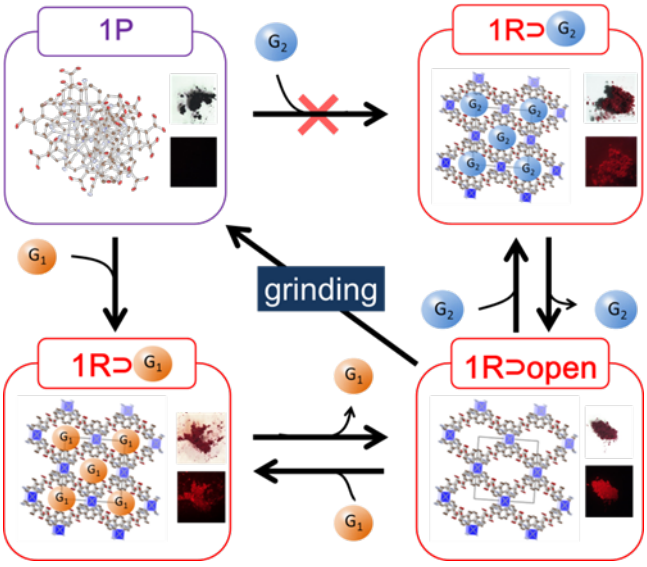

Scheme 2 Schematic diagram showing the shape-memory behavior of complex **1** based on the vapor-adsorption amorphous–crystalline and grinding-driven crystalline–amorphous transformations. Photographs shown in each scheme were taken under ambient white light (top) and light irradiation at 533 nm [bottom, a long-pass filter (λ > 570 nm) was used].

Thermochromic luminescence

Many Pt(II) complexes with effective metallophilic interaction are known to exhibit temperature-dependent luminescence.[14] Since the red crystalline form, **1R⊃water**, also features effective metallophilic interactions, the luminescence properties are expected to be highly dependent on temperature. In addition, as mentioned in the crystal structure section, H_2dcphen has a more expanded π-conjugated electronic system than H_2dcbpy, suggesting that the π-π interaction is more effective. To examine the effects of expanding π-conjugation on the thermochromic luminescence behavior, we examined the temperature dependences of both the luminescence spectrum and crystal structure. Figure 8(a) shows the temperature dependence of the at 740 nm at 100 K, which is at a 17 nm longer wavelength than luminescence spectra of both **1R⊃water** and **2R⊃water**. The red crystalline form, **1R⊃water**, exhibited the ^{3}MMLCT phosphorescence band at 723 nm (1.72 eV) at 100 K; this band

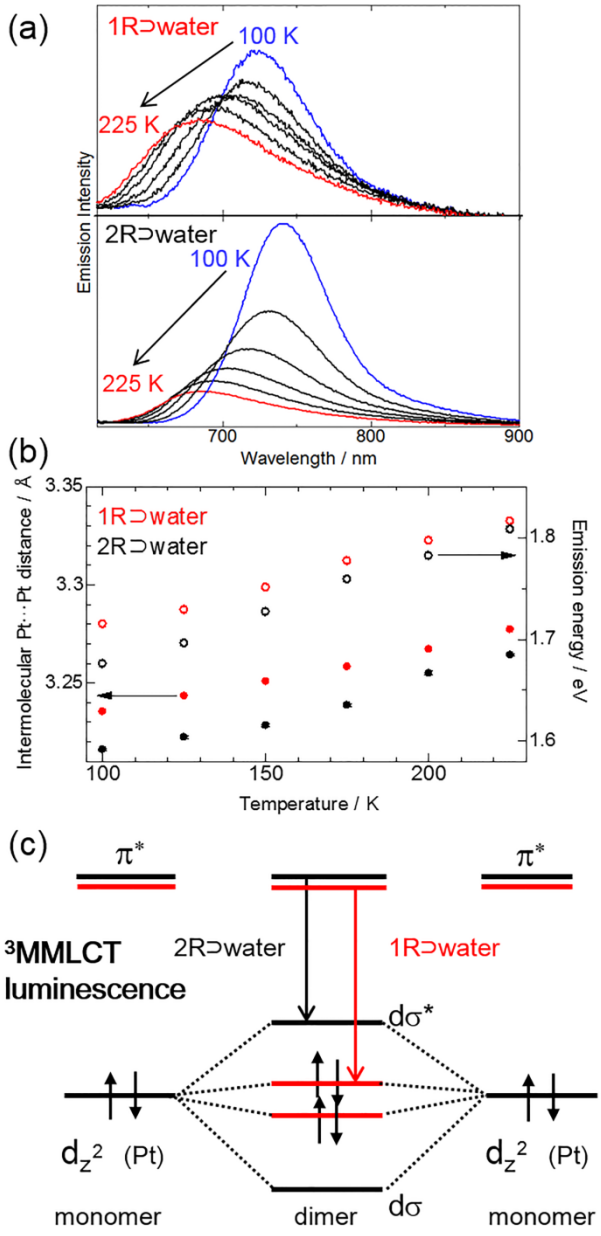

Fig. 8 (a) Temperature dependence luminescence spectra (λ_{ex}= 400 nm) of **1R⊃water** (top) and **2R⊃water** (bottom) from 100 K (blue line) to 225 K (red line). (b) Temperature dependence of the Pt–Pt distances (closed circles) and luminescence energies (open circles) of **1R⊃water** (red) and **2R⊃water** (black). The Pt–Pt distances were estimated by single crystal X-ray structural analysis. (c) Schematic luminescence energy diagrams of **1R⊃water** (red) and **2R⊃water** (black).

shifted to a shorter wavelength with increasing temperature up to 683 nm (1.84 eV) at 225 K. On the other hand, the bipyridine complex, **2R⊃water**, exhibited the same phosphorescence band that of **1R⊃water** at 100 K, and exhibited a similar wavelength (686 nm, 1.84 eV) as that of **1R⊃water** at 225 K. Therefore, **1R⊃water** exhibits the ^{3}MMLCT phosphorescence at a higher energy than **2R⊃water** in this temperature range. In addition, the temperature dependence of the ^{3}MMLCT band energy of **1R⊃water** is smaller than that of **2R⊃water**. In order to clarify the origin of these differences, the temperature dependences of the intermolecular Pt···Pt distances of these two complexes were estimated from the single crystal X-ray diffraction measurement. The crystallographic parameters at each temperature are summarized in Table S1. Single crystal X-ray diffraction analysis was conducted using the same single crystal at various temperatures. Figure 8(b) shows the temperature dependences of the energy of the ^{3}MMLCT band and intermolecular Pt···Pt distances of **1R⊃water** and **2R⊃water**. The intermolecular Pt···Pt distance of **1R⊃water** expended from 3.2355(3) Å at 100 K to 3.2768(8) Å upon a temperature increase to 225 K, whereas the Pt···Pt distance of **2R⊃water** (3.2161(6) Å) was 0.019 Å shorter than that of **1R⊃water** at 100 K and expanded to a similar distance (3.2642(6) Å) as that of **1R⊃water** at 225 K. The difference of the temperature dependence of the intermolecular Pt···Pt distance of **1R⊃water** and **2R⊃water** is in good agreement with the temperature dependences of the ^{3}MMLCT band energy of these complexes: **1R⊃water** exhibited higher-energy phosphorescence and less temperature dependence than **2R⊃water** because of the weaker intermolecular Pt···Pt interactions and their smaller dependence on temperature. It is noteworthy that the cell lengths along the *c* axis corresponding to the direction of the intermolecular Pt···Pt interactions of these complexes are very similar in this temperature range (Figure S13(c)); this result implies that the difference in the molecular shapes of the H_2dcphen and H_2dcbpy ligands does not affect the thickness of the square-planar Pt(II) complex molecule. Consequently, the weaker intermolecular Pt···Pt interactions of **1R⊃water** than those of **2R⊃water** likely originated from the more distorted Pt···Pt stacking structure. In fact, the Pt···Pt···Pt stacking angle of **1R⊃water** is smaller than that of **2R⊃water** in this temperature range (Figure S13(d)). Moreover, in spite of longer Pt···Pt distances of **1R⊃water** than **2R⊃water**, the distances between diamine and cyanide ligands are almost same (Table S2). These are partially caused by the more expanded π-conjugated ligand in **1** than in **2**, *i.e.*, the H_2dcphen ligand may enhance the intermolecular π–π stacking interactions between the diimine and cyanide ligands, resulting in the weaker intermolecular Pt···Pt interactions and higher-energy emission band of **1R⊃water** as compared to those of **2R⊃water** (Figure 8c).

Conclusions

We successfully synthesized a new Pt(II)-diimine complex, $[Pt(CN)_2(H_2dcphen)]$ (**1**; H_2dcphen = 4,7-dicarboxy-1,10-phenanthroline), and found that it shows the unique vapochromic behavior with the vapor-history sensing and ON-OFF-switching functions derived from the shape-memory behavior of the porous framework. The crystal structure is isomorphic to the bipyridine analog, $[Pt(CN)_2(H_2dcbpy)]$ (**2**; H_2dcbpy = 4,4'-dicarboxy-2,2'-bipyridine), and has a similar porous structure. The purple amorphous form of the complex, **1P**, showed drastic color/luminescence changes under exposure to several alcoholic vapors. These vapor-induced color/luminescence changes from **1P** originated from a structural

transformation to red crystalline **1R⊃vapor**, which contains adsorbed vapor molecules in the porous channels. A noteworthy difference between **1P** and **2P** was observed under exposure to *t*-BuOH vapor: Only **2P** showed a drastic color change from purple to red, suggesting that the pores of **1R** are too small to adsorb *t*-BuOH vapor. Interestingly, the crystalline porous structures of both **1R⊃vapor** and **2R⊃vapor** constructed by vapor adsorption were retained after thermal removal of the vapor molecules to form the vapor-free phase, **1R⊃open** and **2R⊃open**, respectively, although the color/luminescence changed because of change in the intermolecular metallophilic interactions. These vapor-free phases can be collapsed by manual grinding in a mortar to regenerate the initial purple amorphous form, **1P** and **2P**. The temperature dependences of the luminescence spectra of **1R** indicated that the luminescence of **1R** was caused by ^{3}MMLCT (metal-metal-to-ligand charge transfer) emission similar to in **2R**; however, the weaker dependence of **1R** may be due to enhanced intermolecular π–π stacking interactions caused by the more expanded π-conjugation of H_2dcphen than that of H_2dcbpy, which would compete with the intermolecular Pt···Pt interactions. These results clearly indicate that the Pt(II)-diimine supramolecular system such as **1** and **2** is not only *multichromic* materials that respond to various external stimuli but also a new type of *vapor-history* sensing materials with ON–OFF switching functions based on the shape memory ability derived from the formation and collapse of the porous structure by vapor adsorption and manual grinding, respectively. Further study on molecule-based shape-memory behavior is currently in progress.

Experimental Section

General Procedures.

All commercially available starting materials were used without purification. The starting materials, $Pt(CN)_2$,[8] the amorphous purple form of the bipyridyl complex ([$Pt(CN)_2(H_2dcbpy)$][8] (**2P**)), and the red crystalline solid of [$Pt(CN)_2(H_2dcbpy)$]·$3H_2O$ (**2R⊃water**) were prepared according to previously published methods. H_2dcphen was synthesized via 4,7-diformyl-1,10-phenanthroline,[15] and the final oxidation step was conducted according to the synthetic procedure of 2,2':6',2''-terpyridine-4'-carboxylic acid using $AgNO_3$.[16] ^{1}H NMR spectra of the samples were measured using a JEOL EX-270 NMR spectrometer at room temperature. Elemental analysis was conducted at the Analysis Center at Hokkaido University.

Synthesis of Purple [$Pt(CN)_2(H_2dcphen)$] (1P)

Yellowish green $Pt(CN)_2$ powder (273 mg, 1.1 mmol) was first suspended in aq. NH_3 (25 mL) followed by the addition of white H_2dcphen powder (134 mg, 0.5 mmol). The reaction mixture was refluxed at 110 °C for one day. After cooling to room temperature, aq. NH_3 (30 mL) was added to the reaction mixture, which was then refluxed for an additional day. After cooling to room temperature, the resultant yellowish green suspension was collected by filtration. Dilute aq. HCl (5 mL) was added to the obtained yellow filtrate to promote precipitation of a purple solid, which was collected by centrifugation. The purple solid was suspended in 3% aq. HCl (200 mL), and the mixture was heated to 100 °C for 10 min. The insoluble precipitates were immediately collected via filtration and dried *in vacuo* to give the desired product in the amorphous purple form (**1P**). Yield: 139 mg, 50%. Elemental analysis calculated for $C_{16}H_8N_4O_4Pt\cdot 2H_2O$: C 35.85, H 2.19, N 10.16. Found: C 35.93, H 2.04, N 10.45. ^{1}H NMR (4% NaOD in D_2O): δ 9.08 (d, 2H), 8.36 (s, 2H), 7.95 (d, 2H).

Red Crystalline Solid of [$Pt(CN)_2(H_2dcphen)$]·$3H_2O$ (1R⊃water)

Purple amorphous solid **1P** (10.6 mg, 0.02 mmol) was dissolved in MeOH (1 mL) containing 120 μL of 10% MeOLi/MeOH solution. H_2O (1.3 mL) was then added to this solution. Diffusion of CH_3COOH vapor into the MeOH-water solution gave red crystals of **1R⊃water** that were suitable for X-ray diffraction analysis.

Preparation of vapor exposed sample

The small amount of the sample (ca. 2 mg) was put into the small glass vial and the vial was placed in the larger capped glass vial with a small amount of liquid (ca. 1 mL) as the vapor source (see Figure S14). The glass vial was stood in the temperature-controlled incubator at 303 K for several days.

Powder X-Ray Diffraction

Powder X-ray diffraction was conducted using either a Rigaku SPD diffractometer at beamline BL-8B at the Photon Factory, KEK, Japan or a Bruker D8 Advance diffractometer equipped with a graphite monochromator using Cu Kα radiation and a one-dimensional LinxEye detector. The wavelength of the synchrotron X-rays was 1.5385(1) Å.

Luminescence Properties

The luminescence spectra of the complexes were measured using a JASCO FP-6600 spectrofluorometer at room temperature. The typical slit widths of the excitation and emission light were 5 and 6 nm, respectively. Temperature-dependent luminescence spectra were measured using a Hamamatsu multichannel photodetector (PMA-11) and a nitrogen laser for the 337 nm excitation. A liquid nitrogen cryostat (Optistat-DN optical Dewar and ITC-503 temperature controller, Oxford Instruments) was used for temperature control.

Vapor Adsorption Isotherms

Vapor adsorption isotherms of the complexes were measured using BELSORP-max vapor adsorption isotherm measurement equipment at 298 K.

Single Crystal X-Ray Diffraction Measurements

All the measurements of **1R⊃water** were conducted using a Rigaku AFC-11 diffractometer with a Mercury CCD area detector at beamline PF-AR NW2A at the Photon Factory, KEK, Japan. The wavelength of the synchrotron X-rays was 0.6890(1) Å. Temperature-dependent measurements of **2R ⊃ water** were conducted using a Rigaku Mercury CCD diffractometer with monochromated Mo Kα radiation (λ=0.71069 Å) and a sealed X-ray tube generator. All single crystals were mounted on a MicroMount coated with paraffin oil. The crystal was then cooled using an N_2 flow–type temperature controller. Diffraction data were collected and processed using CrystalClear software.[17] Structures were solved with the direct method using SIR-2004.[18] Structural refinements were conducted by the full-matrix

least-squares method using SHELXL-97.[19] Non-hydrogen atoms were refined anisotropically, and all hydrogen atoms were refined using the riding model. All calculations were conducted using the Crystal Structure crystallographic software package.[20] The crystallographic data for **1R⊃water** is summarized in Table S1 in comparison with those of **2R⊃water**. Full crystallographic data were deposited with the Cambridge Crystallographic Data Centre (CCDC 1411618 and 1415892-1415902)

Acknowledgements

This work is supported by JST-PRESTO, Grant-in-Aid for Scientific Research on Innovative Area “Artificial Photosynthesis” (No. 2406), (B)(23350025) and (C)(26410063) from MEXT, Japan.

Notes and references

[1] (a) L. Prodi, F. Bolletta, M. Montalti, N. Zaccheroni, *Coord. Chem. Rev*, **2000**, *205*, 59. (b) M. H. Keefe, K. Benkstein, J. T. Hupp, *Coord. Chem. Rev*, **2000**, *205*, 201. (c) M. Kato, *Bull. Chem. Soc. Jpn*, **2007**, *80*, 287. (d) X. Zhang, B. Lin, Z. H. Chen, Z. N. Chen, *J. Mater. Chem*, **2012**, *22*, 11427. (e) O. S. Wenger, *Chem. Rev,* **2013**, *113*, 3686. (f) A. Kobayashi, M. Kato, *Eur. J. Inorg. Chem,* **2014**, 4469.

[2] Neutral Pt(II) complexes: (a) C. E. Buss, K. R. Mann, *J. Am. Chem. Soc*, **2002**, *214*, 1031. (b) J. Ni,Y. H. Wu, X. Zhang, B. Li, L. Y. Zhang, Z. N. Chen, *Inorg. Chem*, **2009**, *48*, 10202. (c) J. Ni,X. Zhang,Y. H. Wu, L. Y. Zhang, Z. N. Chen, *Chem. Eur. J*, **2011**, *17*, 1171. (d) J. Ni, X. Zhang, N. Qiu, Y. H. Wu, L. Y. Zhang, J. Zhang, Z. N. Chen, *Inorg. Chem*, **2011**, *50*, 9090. (e) X. Zhang, J. Y. Wang, J. Ni, L. Y. Zhang, Z. N. Chen, *Inorg. Chem*, **2012**, *51*, 5569. (f) A. Kobayashi, Y. Fukuzawa, H.-C. Chang, M. Kato, *Inorg. Chem*, **2012**, *51*, 7508. (g) S. J. Choi, J. Kuwabara, Y. Nishimura, T. Arai, T. Kanbara, *Chem. Lett*, **2012**, *41*, 65. (h) N. Kitani, N. Kuwamura, T. Tsuji, K. Tsuge, T. Konno, *Inorg. Chem*, **2014**, *53*, 1949.

[3] Cationic Pt(II) complexes: (a) L. J. Grove, J. M. Rennekamp, H. Jude, W. B. Connick, *J. Am. Chem. Soc*, **2004**, *126*, 1594. (b) T. J. Wadas, Q. M. Wang, Y. J. Kim, C. Flaschenreim, T. N. Blanton, R. Eisenberg, *J. Am. Chem. Soc*, **2004**, *126*, 16841. (c) P. Du, J. Schneider, W. W. Brennessel, R. Eisenberg, *Inorg. Chem*, **2008**, *47*, 69. (d) L. J. Grobe, A. G. Oliver, J. A. Krause, W. B. Connick, *Inorg. Chem*, **2008**, *47*, 1408. (e) M. L. Muro, C. A. Daws, F. N. Castellano, *Chem. Commun*, 2008, 6134. (f) A. Kobayashi, T. Yonemura, M. Kato, *Eur. J. Inorg. Chem.* **2010**, 2465. (g) C. S. Lee, R. R. Zhuang, S. Sabiah, J. C. Wang, W. S. Hwang, I. J. B. Lin, *Organometallics*, **2011**, *30*, 3897. (h) A. Han, P. Du, Z. Sun, H. Wu, H. Jia, R. Zhang, Z. Liang, R. Cao, R. Eisenberg, *Inorg. Chem*, **2014**, *53*, 3338.

[4] Anionic Pt(II) complexes: J. Forniés, S. Fuertes, J. A. López, A. Martín, V. Sicilia, *Inorg. Chem*. **2008**, *47*, 7166.

[5] Double salt Pt(II) complexes: (a) C. L. Exstrom, J. R. Sowa, Jr., C. A. Daws, D. Janzen, K. R. Mann, *Chem. Mater*, **1995**, *7*, 15. (b) C. A. Daws, C. L. Exstrom, J. R. Sowa, Jr., K. R. Mann, *Chem. Mater*, **1997**, *9*, 363. (c) C. L. Exstrom, M. K. Pomije, K. R. Mann, *Chem. Mater*, **1998**, *10*, 942. (d) C. L. Exstrom, M. K. Pomije, K. R. Mann, *Chem. Mater*, **1998**, *10*, 942. (e) S. M. Drew, L. I. Smith, K. A. McGee, K. R. Mann, *Chem. Mater*, **2009**, *21*, 3117.

[6] Dinuclear Pt(II) complexes: (a) M. Kato, A. Omura, A. Toshikawa, S. Kishi, Y. Sugimoto, *Angew. Chem. Int. Ed*, **2002**, *41*, 3183. (b) S. C. F. Kui, S. S. Y. Chui, C. M. Che, N. Zhu, *J. Am. Chem. Soc*, **2006**, *128*, 8297.

[7] Other complexes: (a) L. G. Beauvais, M. P. Shores, J. R. Long, *J. Am. Chem. Soc*, **2000**, *122*, 2763. (b) J. Lefebvre, R. J. Batchelor, D. B. Leznoff, *J. Am Chem. Soc*, **2004**, *126*, 16117. (c) G. M. Espallargas, L. Brammer, J. van de Streek, K. Shankland, A. J. Florence, H. Adams, *J. Am. Chem. Soc*, **2006**, *128*, 9584. (d) N. Baho, and D. Zargarian, *Inorg. Chem*, **2007**, *46*, 299. (e) E. J. Fernández, J. M. López-de-Luzuriaga, M. Monge, M. E. Olmos, R. C. Puelles, A. Laguna, A. A. Mohamed, J. P. Fackler, Jr., *Inorg. Chem*, **2008**, *47*, 8069. (f) B. Li, R. J. Wei, J. Tao, R. B. Huang, L. S. Zheng, Z. Zheng, *J. Am. Chem. Soc*, **2010**, *132*, 1558. (g) C. E. Strasser, V. J. Catalano, *J. Am. Chem. Soc*, **2010**, *132*, 10009. (h) Y. J. Li, Z. Y. Deng, X. F. Xu, H. B. Wu, Z. X. Cao, Q. M. Wang, *Chem. Commun*, **2011**, *47*, 9179.

[8] M. Kato, S. Kishi, Y. Wakamatsu, Y. Sugi, Y. Osamura, T. Koshiyama, M. Hasegawa, *Chem Lett*, **2005**, *34*, 1368.

[9] (a) J. Van Humbeeck, *Adv. Eng. Mater*, **2001**, *3*, 837. (b) M. Behl, M. Y. Razzaq, A. Lendlein, *Adv. Mater*, **2010**, *22*, 3388. (c) T. Xie, *Polymer*, **2011**, *52*, 4985.

[10]Y. Sakata, S. Furukawa, M. Kondo, K. Hirai, N. Horike, Y. Takashima, H. Uehara, N. Louvain, M. Meilikhov, T. Tsuruoka, S. Isoda, W. Kosaka, O. Sakata, S. Kitagawa, *Science,* **2013**, *339,* 193.

[11] The stability of **1R⊃EtOH** in air was checked by ^{1}H NMR spectroscopy (see Figure S15), and the adsorbed EtOH in **1R⊃EtOH** could be remained at least 1 night.

[12] **1R⊃EtOH** was also converted to the intial **1P** by manual grinding in a mortar at room temperature.The detail is now under investigation.

[13] H. L. Goderis, B. L. Fouwe, S. M. Van Cauwebergh, P. P. Tobback, *Anal. Chem.* **1986**, *58*, 1561.

[14] (a) V. H. Houlding, V. M. Miskowski, *Coord. Chem. Rev.*, **1991**, *111*, 145. (b) G. Gliemann, H. Yersin, *Sruct. Bonding*, **1985**, *62*, 87. (c) W. B. Connick, L. M. Henling, R. E. Marsh, H. B. Gray, *Inorg. Chem.*, **1996**, *35*, 6261. (d) M. Kato, C. Kosuge, K. Morii, J. S. Ahn, H. Kitagawa, T. Mitani, M. Matsushita, T. Kato, S. Yano, M. Kimura, *Inorg. Chem.*, **1999**, *38*, 1638.

[15] M. Yanagida, L. P. Singh, K. Sayama, K. Hara, R. Katoh, A. Islam, H. Sugihara, H. Arakawa, M. K. Nazeeruddin, M. Grätzel, *J. Chem. Soc., Dalton Trans*, **2000**, 2817.

[16] H. Wolpher, S. Sinha, J. Pan, A. Johansson, M. J. Lundqvist, P. Persson, R. Lomoth, J. Bergquist, L. Sun, V. Sundström, B. Akermark, T. Polivka, *Inorg. Chem,* **2007**, *46*, 638.

[17] *CrystalClear*; Molecular Structure Corporation: Orem, UT, 2001.

[18] SIR2004: M. C. Burla, R. Caliandro, M. Camalli, B. Carrozzini,G. L. Cascarano, L. De Caro, C. Giacovazzo, G. Polidori, R. Spagana, *J. Appl. Crystallogr.* **2005**, *38*, 381.

[19] SHELX97; G. M. Sheldrick, *Acta Crystallogr., Sect. A* **2008**, *64*, 112.

[20] *CrystalStructure 3.7.0*, Crystal Structure Analysis Package; Rigaku and Rigaku/MSC, 2000–2005.

Entry for the Table of Contents (Please choose one layout)

Layout 1:

FULL PAPER

New molecule-based shape memory behavior of a newly synthesized Pt(II)-complex, $[Pt(CN)_2(H_2dcphen)]$ (**1**; H_2dcphen = 4,7-dicarboxy-1,10-phenanthroline), is reported. Three dimensional flexible network structure constructed by one-dimensional intermolecular Pt-Pt interaction and two dimensional hydrogen bonds enables it to exhibit not only vapor-history sensing function, but also ON-OFF switching of vapor sensing function.

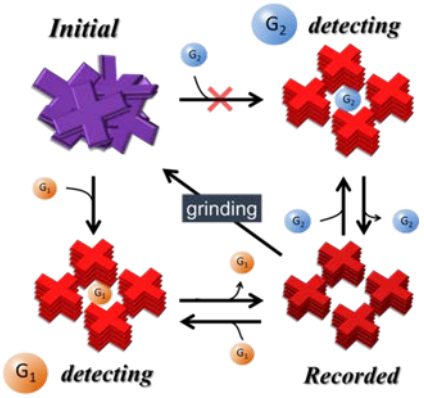

Yasuhiro Shigeta, Atsushi Kobayashi, Tadashi Ohba, Masaki Yoshida, Takeshi Matsumoto, Ho-Chol Chang, and Masako Kato**

Page No. – Page No.

Shape-memory Platinum(II) Complexes: Intelligent Vapor-History Sensor with ON-OFF Switching Function